Cellular and Molecular Life Sciences (2025) 82:28
https://doi.org/10.1007/s00018-024-05541-4

ORIGINAL ARTICLE

HFM1 is essential for the germ cell intercellular bridge transport in primordial follicle formation in mice

Yuheng He[1] · Huiyuan Wang[1] · Tongtong Hong[1] · Luanqian Hu[1] · Chao Gao[1] · Li Gao[1] · Yugui Cui[1] · Rongrong Tan[1] · Danhua Pu[1] · Jie Wu[1]

Received: 1 September 2024 / Revised: 11 November 2024 / Accepted: 5 December 2024
© The Author(s) 2024

Abstract

The reproductive lifespan of female mammals is determined by the size of the primordial follicle pool, which comprises oocytes enclosed by a layer of flattened pre-granulosa cells. Oocyte differentiation needs acquiring organelles and cytoplasm from sister germ cells in cysts, but the mechanisms regulating this process remain unknown. Previously helicase for meiosis 1 (HFM1) is reported to be related to the development of premature ovarian insufficiency. Here, it is found that HFM1 is involved in oocyte differentiation through organelle enrichment from sister germ cells. Further study indicates that HFM1 is involved in intercellular directional transport through intercellular bridges via the RAC1/ANLN/E-cad signaling pathway, which is indispensable for oocyte differentiation and primordial follicle formation. These findings shed light on the critical role of HFM1 in intercellular bridge transport, which is essential for the establishment of the primordial follicle pool and presenting new horizons for female fertility protection.

Keywords HFM1 · Intercellular bridge · Oocyte differentiation · POI · Primordial follicle formation

Introduction

The total number of primordial follicles is derived from primordial germ cells (PGCs) in fetal gonads, which serve as the ovarian reserve. This non-growing population of the primordial pool is critical for long-term ovulation and fertility in females [1]. Premature ovarian insufficiency (POI) is a clinical syndrome of ovarian dysfunction, defined as cessation of menstruation before 40 years of age [2]. Theoretically, the abnormality or failure of primordial follicle formation is closely related to POI [3, 4]. We previously identified that HFM1 (helicase for meiosis 1), also known as MER3, POF9, Si-11, SEC63D1, and Si-11-6, is a candidate gene of POI [5, 6]. HFM1 was reported to be mainly expressed in germline cells, which is required for crossover formation and complete synapsis of homologous chromosomes in spermiogenesis [7]. Our previous research also found that *Hfm1* gene conditional knockout (*Hfm1*-cKO) mice exhibit symptoms of POI with a decreasing number of primordial follicles [8]. However, the underlying mechanism remains largely unknown.

In female mice, the process of primordial follicle formation begins when PGCs proliferate with incomplete cytokinesis from embryonic day (E) 10.5 to E14.5. Sister germ cells derived from a single progenitor remain connected by stable intercellular bridges (ICBs), forming germline cysts and then undergoing meiosis [9, 10]. The number of germ cells peaks around E14.5 (about 20,000 germ cells per ovary) and starts to decline afterward. Interestingly, germ cells with three or four intercellular bridges have priority to receive organelles and cytoplasm to become primary oocytes, and these germ cells seem to be preferentially protected from cell death by acquiring cellular content from sister germ cells between E14.5 and E17.5. Germ cell number drops rapidly

Yuheng He and Huiyuan Wang contributed equally to this work.

✉ Rongrong Tan
tanrongrong86119@163.com

✉ Danhua Pu
pudanhua@139.com

✉ Jie Wu
wujiemd@126.com

[1] State Key Laboratory of Reproductive Medicine and Offspring Health, Department of Obstetrics and Gynecology, The First Affiliated Hospital of Nanjing Medical University/ Jiangsu Province Hospital/Jiangsu Women and Children Health Hospital, Nanjing 210036, China

Published online: 27 December 2024

following intercellular bridge detached and cyst fragmentation from E17.5 to postnatal day (P) 0. Ultimately, only ~ 15 to 20% of germ cells differentiate into primary oocytes and are surrounded by the presumptive granulosa cells to form the primordial follicle by P3, while the remaining fetal germ cells undergo programmed cell death after donating these materials [11–13].

To investigate the potential importance of HFM1 for primordial follicle formation, we have observed oocyte development of HFM1 knockout female mice during the late embryonic to early postnatal period. It was found that HFM1 was associated with organelle and cytoplasmic transport via intercellular bridges between sister germ cells. Therefore, a hypothesis was proposed that HFM1 could regulate the structure and function of the intercellular bridge in female germline cysts through RAC1/ANLN/E-cad signaling pathway, interfere with the selection of primary oocytes, and affect the formation of primordial follicles, which participated in the pathogenesis of POI. Our results gain a new insight into the mechanisms of germ cell selection and primordial follicle formation.

Materials and methods

Mice

Mice carrying a floxed (loxP-flanked) allele of *Hfm1* (*Hfm1*$^{flox/wt}$) were produced from GemPharmatech Co., Ltd. (Nanjing, China), which has been described in detail previously [8]. These mice were maintained on identical C57BL/6J genetic background. *Hfm1*$^{flox/wt}$ mice were crossed with *Gdf9-Cre*$^{+}$ mice to produce *Hfm1*$^{flox/flox}$*Gdf9-Cre*$^{+}$ mice as *Hfm1* cell-conditional KO (*Hfm1*-cKO). Then, *Hfm1*$^{flox/flox}$*Gdf9-Cre*$^{+}$ female mice were mated with *Hfm1*$^{flox/null}$*Gdf9-Cre*$^{-}$ male mice to obtain *Hfm1*$^{null/null}$ (*Hfm1*-KO) female mice (Fig. 1b), and wild-type (WT) mice were used as the control.

Mice were housed under specific pathogen-free (SPF) conditions with controlled lighting (12 h light-dark cycle) and temperature (22–26 °C) and allowed free access to water and food. Female mice were mated with males overnight and checked for a vaginal plug the following morning. The presence of a vaginal plug was confirmed to embryonic day (E) 0.5. The day of postpartum was considered to be the postnatal day (P) 1. All mice experiments were approved by the Committee on the Ethics of Animal Experiments of Nanjing Medical University (IACUC 2303011).

Each mouse was cut a small tail snip for DNA extraction using the mouse genotyping kit (PD101; Vazyme, China). PCR reactions were completed using primer sequences listed in Table S1. PCR products were performed by DNA agarose gel electrophoresis to check the genotypes.

Antibodies

The antibodies used for immunofluorescence analysis and Western blotting are listed in Table S2.

Histology, immunofluorescence and follicle counts

Paraffin-embedded samples: Ovaries were fixed in 4% paraformaldehyde (PFA) in pre-chilled phosphate-buffered saline (PBS) overnight at 4 °C, then transferred to 70% ethyl alcohol, dehydrated, infiltrated with paraffin wax, and sliced into 4-μm-thick sections. The ovarian sections were deparaffinized and stained with hematoxylin. For immunofluorescence, ovarian tissues were deparaffinized, rehydrated, and subjected to antigen retrieval using a citrate antigen retrieval solution (P0081; Beyotime, China). Then, sections were washed in PBS and blocked (P0260; Beyotime, China) for 30 min at room temperature. Primary antibodies were incubated in a wet box overnight at 4 °C. After washing with PBS, the samples were reacted with secondary antibodies labeled with Alexa 488, 594, (Proteintech Group, China) for 60 min at room temperature. The sections were then stained with Hoechst 33,342 (1:200, H3570; Invitrogen, USA) for 30 min, and sealed in antifade mounting medium (P0126; Beyotime, China) with coverslips. The images were acquired on a fluorescence microscope (Nikon, Japan) and the NIS-Elements BR 5.2 software.

The whole ovaries were sequentially sliced and stained with DDX4. Germ cells were counted on every five sections. To estimate the total number of germ cells in each ovary, the sum was multiplied by five. The germ cells area, γ-tubulin and APT5A1 foci area were measured using ImageJ software.

Transmission electron microscopy

Fresh ovaries were obtained from *Hfm1*-KO and WT mice and fixed with 2.5% normal glutaraldehyde in PBS. After being dehydrated in gradient alcohol and embedded at room temperature, ultrathin sections of tissues were collected on formvar-coated grids and examined with transmission electron microscopy (JEM-1400Flash; JEOL, Japan).

Cell culture and drug treatment

The human embryonic kidney cell line 293T (HEK293T) cells were cultured in Dulbecco's modified Eagle medium/nutrient mixture F-12 (ZQ-600; Zhong Qiao Xin Zhou, China) with 10% fetal bovine serum (Yeason, China), 1%

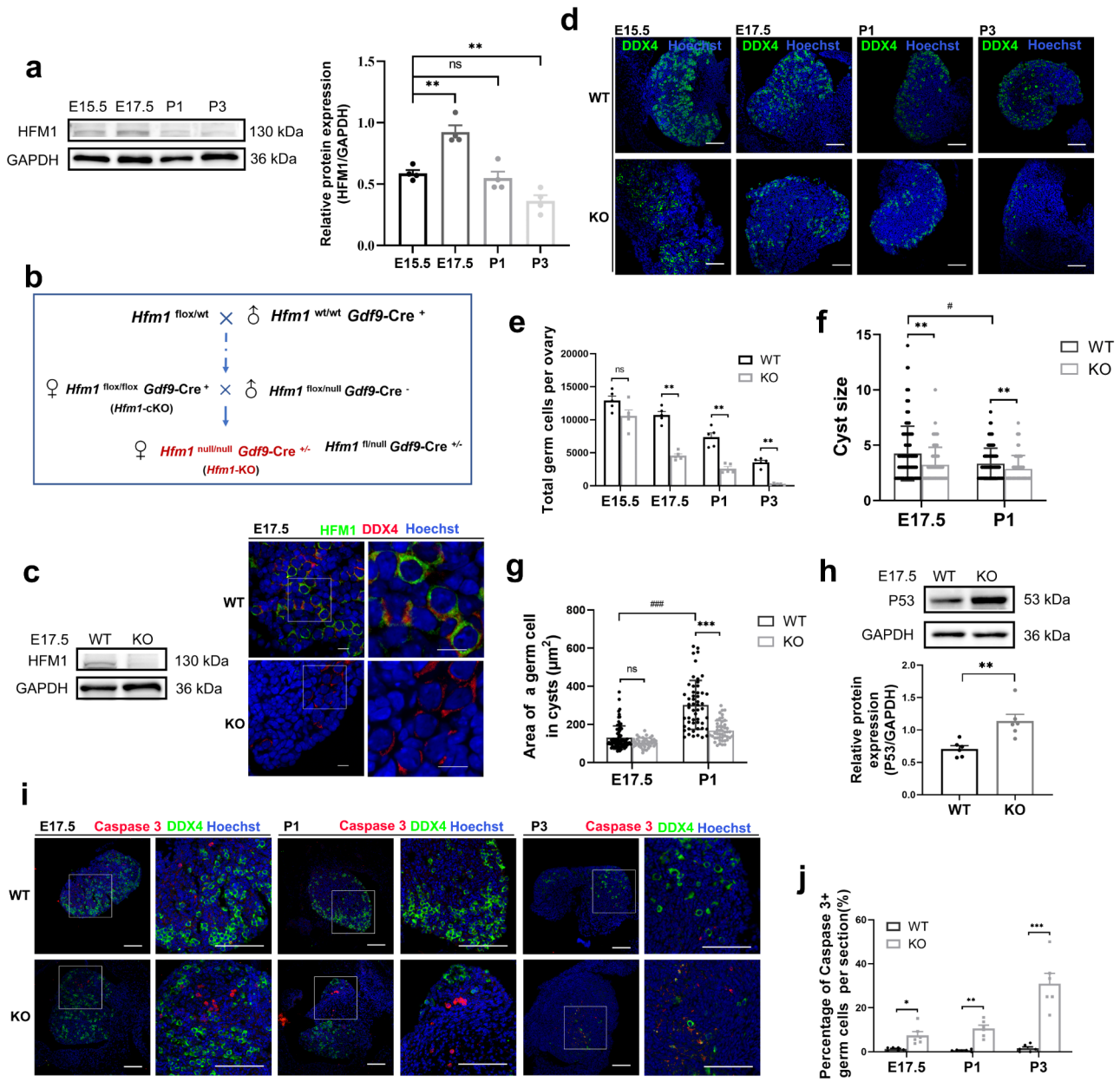

Fig. 1 HFM1 was indispensable for primordial follicle formation. **a** Western blotting analysis of HFM1 expression patterns in the mouse ovaries from E15.5 to P3 (unpaired Student's t-test, $n=4$ independent experiments, ** $P=0.001$ or ** $P=0.005$ vs. E15.5). GAPDH served as a loading control. The protein level of HFM1 increased markedly at E17.5. **b** Breeding scheme to achieve *Hfm1*-KO female mice. **c** Western blotting analysis showed the complete deletion of HFM1 protein in E17.5 *Hfm1*-KO ovaries. **d** Immunofluorescence staining with germ cell marker DDX4 (green) in E15.5, E17.5, P1 and P3 ovaries. Hoechst (blue) was used to identify the nuclear DNA. Scale bars: 100 μm. **e** Quantitative analysis of germ cell count is shown for WT and *Hfm1*-KO ovaries at E15.5, E17.5, P1, and P3 (unpaired Student's t-test, $n=5$ animals for each genotype, *** $P<0.001$ vs. WT). **f** The number of germ cells (cyst size) in cysts in E17.5 ($n=118$ for WT and $n=71$ for KO) and P1 ovaries ($n=91$ for WT and $n=65$ for KO) (Mann-Whitney U test, ** $P=0.003$ or 0.009 vs. WT, $^{\#}P=0.015$ vs. E17.5). **g** The area of the germ cell in cysts at E17.5 ($n=81$ for WT and $n=41$ for KO) and P1 ($n=53$ for WT and $n=46$ for KO) (Mann-Whitney U test, *** $P<0.001$ vs. WT, $^{\#\#\#}P<0.001$ vs. E17.5). **h** Western blotting was performed to examine the level of P53 in E17.5 ovaries. The level of P53 was higher in the *Hfm1*-KO than in the WT ovaries (unpaired Student's t-test, $n=6$ independent experiments, ** $P=0.004$ vs. WT). **i** E15.5, E17.5, P1, and P3 ovaries were stained with germ cell marker DDX4 (green), apoptotic signal Caspase 3 (red). Hoechst (blue) was used to identify the nuclear DNA. Scale bars: 100 μm. **j** The number of apoptotic cells (Caspase3-positive signals) per section increased significantly in *Hfm1*-KO ovaries (unpaired Student's t-test, $n=6$, * $P=0.015$, ** $P=0.001$, *** $P<0.001$ vs. WT). Data are presented as mean ± SEM. ns: no significant difference

penicillin-streptomycin solution incubating in a 37 °C incubator with 5% CO_2. Rac1-specific inhibitor NSC23766 (HY-15723; MCE, USA) was dissolved in DMSO. The concentration of NSC23766 was 100 μM for 24 h in HEK293T cells. The control group was supplemented with the same volume of DMSO.

Lentiviral transfection

A lentiviral packaging system was used to achieve *HFM1* overexpression (*HFM1*-OE). HEK293T was chosen for its negligible expression of HFM1 and efficient transfected. HEK293T cells were grown to 80% confluency and infected with lentiviral vectors targeting HFM1 or with negative control. After 24 h, the supernatant was removed and replaced with a complete medium. Cell lines with stable overexpression of *HFM1* were obtained by puromycin selection. The pLV4ltr-Puro-CMV-c3×FLAG lentivirus vector (Corues Biotechnology, China) containing a coding sequence of *HFM1* was constructed to achieve *HFM1* overexpression.

Cell counting kit-8

The wild-type, negative control and lentivirus-infected HEK293T cells were plated in 96-well plates (1×10^3 cells each well) and incubated for the indicated time (0, 24, 48, 72 h). Afterward, each well added 10 μL of CCK-8 solution (#K1018; APExBIO, USA) in a light-protected environment at 37 °C for 2 h. The absorbance value of each well was measured at 450 nm using a microplate reader (Thermo Fisher Scientific, USA).

RNA extraction and quantitative real-time PCR (qRT-PCR)

E17.5 ovaries, KGN cells (human granulosa-like tumor cell line), mouse primary granulosa cells and HEK 293T cells were obtained to extracted total RNA by RNA-Quick extraction kit (ES Science, China), and cDNA was synthesized through a PrimeScript RT Reagent Kit (Vazyme, China). cDNA of oocytes was synthesized by single cell sequence specific amplification kit (Vazyme, China). qRT-PCR was performed in 20 μl reactions using a Taq Pro Universal SYBR qPCR Master Mix (Vazyme, China). The primer sequences of the targeted genes are listed in Table S1.

Western blotting

Total proteins were lysed with radioimmunoprecipitation assay lysis buffer (Beyotime, China) containing 1mM phenylmethanesulfonyl fluoride (PMSF). Lysates were centrifuged at 12,000 g at 4 °C for 15 min, and the supernatant was collected and preserved at -80 °C for later use. Protein concentrations were determined using BCA protein assay kit (EpiZyme, China). Proteins lysed in 1 × SDS sample buffer were boiled for 5 min and separated by sodium dodecyl sulfate-polyacrylamide gel electrophoresis (SDS-PAGE) and transferred to the PVDF membrane (Bio-Rad, USA) using a standard protocol. After the membranes were submerged in blocking buffer [5% skim milk in TBST (25 mM Tris, 150 mM NaCl, pH 7.4 and 0.1% Tween-20)] at room temperature for 20 min. The membrane was incubated with primary antibodies and probed with the respective secondary antibodies. Protein expression of GAPDH was used as a loading control. The membrane was exposed and scanned using a super enhanced chemiluminescence (ECL) detection reagent (Yeasen, China). Images were captured using the Tanon 4800 imaging system (China).

Co-immunoprecipitation

Proteins were isolated from lentivirus-infected HEK293T cells or ovarian tissues using NP-40 Lysis Buffer (Beyotime, China) with 1mM PMSF. Next, IP-indicated antibodies (4 μg) or paired IgG (4 μg) were cross-linked to protein A/G magnetic beads (#HY-K0202; MCE, USA). After incubation at 4 °C overnight, the beads were washed with lysis buffer four times. Then, proteins were mixed with beads with antibody cross-linking, and proteins bound to the beads were eluted by sodium dodecyl sulfate (SDS) sample buffer. The precipitated protein complexes were then used for Western blotting as described above.

Ovary isolation and vitro culture

Ovaries were dissected carefully from mice at the designated time in PBS under a stereomicroscope (Nikon, Japan) in sterile conditions. To knock down the *Hfm1* gene, shRNA-*Hfm1* was cloned into hU6-MCS-CMV-EGFP vector. The cDNA sequence of the *Rac1* gene was inserted into the pLV11ltr-Puro-mCherry-CMV vector to overexpress the *Rac1* gene. GeneChem (China) constructed the adenoviral vectors expressing shRNA-*Hfm1* and GFP. Corues Biotechnology (China) constructed the lentiviral vectors expressing RAC1 and mCherry. The ovaries were randomly divided into three groups: the control group, the Ad-shRNA-*Hfm1* group (*Hfm1*-KD), the Ad-shRNA-*Hfm1* + LV-*Rac1* group (*Hfm1*-KD + *Rac1*-OE). The isolated ovaries from E17.5 wild-type fetal mice were cultured for 24 h in a medium supplemented with Ad-shRNA-*Hfm1* or/and LV-*Rac1*-mCherry. After further culture in vector-free media for 4 days, ovaries were either stored at -80 °C for subsequent Western blotting or immediately fixed for immunofluorescence studies.

Statistical analysis

All data are presented as means ± SEM of at least three independent experiments. The statistical tests performed on the data are detailed in the respective figure legends. Unpaired Student's t-test was used to analyze the difference between the two groups. One-way ANOVA combined with Tukey's post hoc test was used to analyze the significance among three or more groups. Mann-Whitney U test was performed in nonnormal data. $p < 0.05$ was considered significant. The following symbols are used throughout the figures to indicate statistical significance: $*P < 0.05$, $**P < 0.01$, $***P < 0.001$. ns: no significant difference.

Results

HFM1 is indispensable for primordial follicle formation in mice

The *Hfm1* gene is located on chromosome 5 in mice, whose expression is restricted to the ovary and testis but not in somatic tissues. The previous results prompted us to investigate the expression patterns of HFM1 during germ cell development in perinatal mouse ovaries. Western blotting analysis demonstrated that the protein levels of HFM1 were consistently up-regulated during the embryonic period rather than postnatal and reached a peak expression level at the E17.5 phase (Fig. 1a). To explore the role of HFM1 in the formation of primordial follicles, we crossed conditioned knockout female mice ($Hfm1^{flox/flox}Gdf9\text{-}Cre^{+}$), in which *Hfm1* gene was knockout in mature oocytes, with heterozygous male mice ($Hfm1^{flox/null}Gdf9\text{-}Cre^{-}$) to obtain HFM1 systematic knockout mice ($Hfm1^{null/null}$) (Fig. 1b).

Correct targeting of *Hfm1* alleles was confirmed by genotyping PCR (Supplementary Fig. 1a). The HFM1 protein was undetected in *Hfm1*-KO ovaries by Western blotting analysis and immunofluorescence (Fig. 1c). The *Hfm1*-KO female mice showed no abnormality in their daily behavior, and their body weights (Supplementary Fig. 1b, c) were similar to those of the wild-type (WT) mice after 1, 2, 3, 4, and 6 weeks of birth. However, the *Hfm1*-KO mice were sterile with invisible ovaries (black straight lines) and a rudimentary uterus (Supplementary Fig. 1d), indicating oogenesis defects in these mice. Histologic analysis revealed severe primordial follicle deficiency in the P1 and P3 ovaries of postnatal mice, but many germ cells still remain in the E15.5 and E17.5 ovaries of embryonic mice (Supplementary Fig. 1e).

To assess whether HFM1 deletion ultimately leads to the reduction of the germ cell population, immunofluorescence was stained with DDX4, a germ cell marker (Fig. 1d). Initially, we found that the quantity of germ cells in E15.5 *Hfm1*-KO mice ovaries was comparable to WT counterparts. However, there was a sharp decrease in E17.5 *Hfm1*-KO mice, and with oocyte differentiation, increasing numbers of germ cells continued to decline. Moreover, the P3 *Hfm1*-KO ovaries had lost almost all germ cells compared to the WT group (Fig. 1e). Asymmetric cell fate in the germline cyst was a highly conserved phenomenon during female gametogenesis. We found that the number of germ cells in cysts was decreased in E17.5 and P1 *Hfm1*-KO mice (Fig. 1f). Additionally, the area of an *Hfm1*-KO germ cell was comparable to that of WT germ cells at E17.5, but was apparently smaller than that in WT mice at the P1 phase (Fig. 1g).

As is well known, only a small fraction (~15 to 20%) of fetal germ cells survive to become primary oocytes, with high levels of perinatal germ cells undergoing cell death in both humans and mice [11, 14, 15]. It is generally accepted that apoptosis is the major mechanism responsible for the depletion of germ cells [16, 17]. To determine the cellular mechanism responsible for germ cell excessive demise in *Hfm1*-KO mice, the ovaries were stained with an antibody against P53 and Caspase 3 to determine the incidence of apoptosis. Compared to WT group, the expression of P53 was relatively higher in E17.5 *Hfm1*-KO ovaries (Fig. 1h), while quantification of the percent of Caspase 3 positive germ cells is significantly greater in *Hfm1*-KO ovaries by immunofluorescence (Fig. 1i, j). These results proved that germ cells which have the potential to become oocytes, were not been protected from cell death in *Hfm1*-KO ovaries.

HFM1 is involved in oocyte differentiation through organelle enrichment from sister germ cells

How cysts support mammalian oocyte production by defining sister germ cells as well as oocytes and which germ cells will be selected to receive organelles and cytoplasm to become primary oocytes remain open questions [14, 18, 19]. Several studies have provided some clues, for example, compared with the sister germ cells, the future oocytes have a larger volume, in which centrosomes, Golgi complexes, endoplasmic reticulum and mitochondria organize into a Balbiani body (B-body) [20, 21]. In our research, oocyte-specific B-bodies were recognized in WT ovaries rather than *Hfm1*-KO ovaries by transmission electron micrographs (Fig. 2a) and immunofluorescence (Fig. 2b). To further examine the intercellular organelle movement in mice cysts, we stained fetal ovarian mitochondria with ATP5A1 (Fig. 2c). Statistical analysis showed that the APT5A1 foci area of the germ cell in cysts was significantly decreased in *Hfm1*-KO mice at E17.5 and P1 (Fig. 2d). Similar results were verified by Western blotting analysis that the expression of ATP5A1 protein was reduced in *Hfm1*-KO ovaries

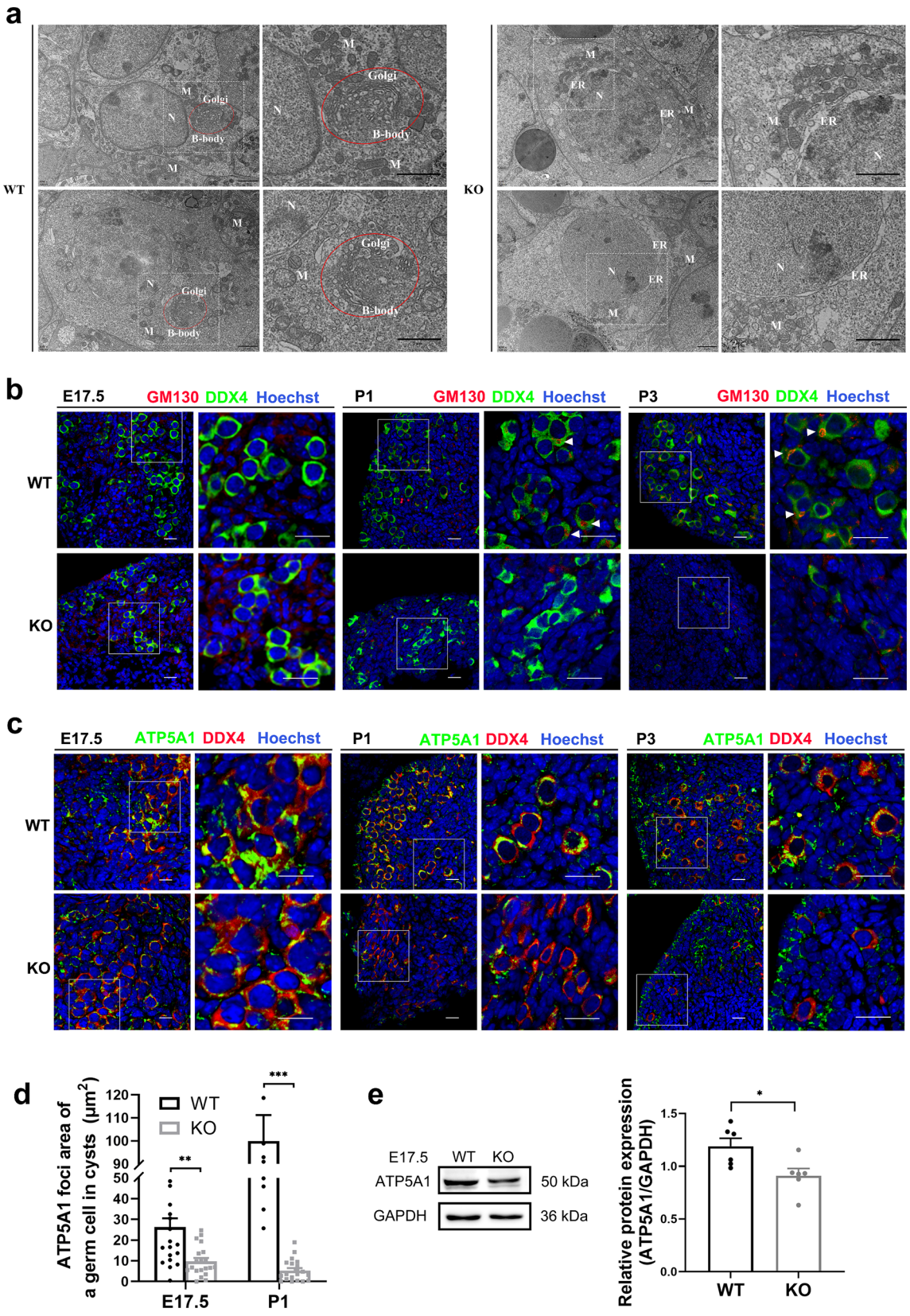
a
WT
KO
M
Golgi
N
B-body
ER
b
E17.5 GM130 DDX4 Hoechst
P1 GM130 DDX4 Hoechst
P3 GM130 DDX4 Hoechst
WT
KO
c
E17.5 ATP5A1 DDX4 Hoechst
P1 ATP5A1 DDX4 Hoechst
P3 ATP5A1 DDX4 Hoechst
WT
KO
d
ATP5A1 foci area of a germ cell in cysts (μm²)
WT
KO
**
***
E17.5
P1
e
E17.5 WT KO
ATP5A1 50 kDa
GAPDH 36 kDa
Relative protein expression (ATP5A1/GAPDH)
*
WT
KO

Fig. 2 Depletion of HFM1 affected organelle enrichment in germline cysts. **a** Transmission electron micrograph of Balbiani body (B-body, red circle) in P1 WT and *Hfm1*-KO mice. Nucleus (N), Mitochondria (M), Endoplasmic reticulum (ER). Scale bars: 2 μm. **b** Immunofluorescence staining for GM130 (red) and DDX4 (green) at E17.5, P1, and P3. The nucleus was stained by Hoechst (blue). GM130 labeled B-body (a large Golgi sphere, white triangle). Scale bars: 20 μm. **c** E17.5, P1 and P3 ovaries were stained with mitochondria marker ATP5A1 (green) and DDX4 (red). Hoechst (blue) was used to identify the nuclear DNA. Scale bars: 20 μm. **d** The ATP5A1 foci area of a germ cell in cysts was generated by ImageJ software at E17.5 and P1 (unpaired Student's t-test, $n=20$, ** $P=0.001$, *** $P<0.001$ vs. WT). *Hfm1*-KO resulted in less distribution of the ATP5A1 foci area. **e** Western blotting analysis of ATP5A1 protein level in E17.5 wild-type and *Hfm1*-KO ovaries (unpaired Student's t-test, $n=6$ independent experiments, * $P=0.022$ vs. WT). Data are presented as mean ± SEM

at E17.5 (Fig. 2e). At P1 and P3, the pericentriolar material stained with pericentrin was not obviously detected in *Hfm1*-KO germ cells (Fig. 3a). Our results suggested the dysfunction of organelle enrichment in *Hfm1*-KO germ cells.

As is known, more extra centrioles, Golgi, mitochondria, and other cytoplasmic components are required in the oocytes which are meant to be primordial follicles. Partitioning-defective Protein 6 (PAR6) could be used as a potential marker of germ cells that differentiated into oocytes [22]. Our results showed that the expression of PAR6 was observed in WT germ cells at E17.5, and became strong in the nuclei of all primordial follicular oocytes at P3. However, the expression of PAR6 in *Hfm1*-KO germ cells progressively declines from E17.5 to P3 (Fig. 3b). *Foxl2* has been considered as a granulosa cell maker gene [23, 24]. Typical primordial follicle consists of a single oocyte surrounding by a layer of FOXL2-positive flat granulosa cells (dash line). Immunofluorescence stained with FOXL2 in mouse ovaries suggested that typical primordial follicle structure was rarely observed in the P3 *Hfm1*-KO ovaries, compared with the WT group (Fig. 3c). Therefore, HFM1 was essential for organelle enrichment from sister germ cells during oocyte differentiation.

HFM1 deletion impacts intercellular bridge formation and stabilization in female germline cysts

Stable intercellular bridges are conserved during gametogenesis in multicellular animals, which are formed as the result of incomplete cytokinesis during mitotic divisions and enable germ cells to exchange organelles and/or macromolecules [18, 25, 26]. Intercellular bridges were observed in E17.5 WT ovaries, but smaller anomalous structures were found in *Hfm1*-KO ovaries by electron micrographs (Fig. 4a). Besides, cytoplasmic materials were observed in the lumen of ICB (red circle), joining two P1 germ cells in WT ovaries, instead of *Hfm1*-KO ovaries, in which the plasma membrane develops large gaps between germ cells (black triangle) and little organelle was observed in cytoplasm of oocytes (Fig. 4b and Supplementary Fig. 2a).

The testis expressed 14 (TEX14) protein is essential in regulating the formation of intercellular bridges [27–29]. the expression level of which was significantly down-regulated in E17.5 *Hfm1*-KO ovaries compared with WT ovaries (Fig. 4c). Stable intercellular bridge formation requires TEX14 disruption of interactions between other cytokinesis components. TSG101 was recruited at the ICBs to orchestrate the final membrane scission [28, 30], and the expression level of which was significantly up-regulated in E17.5 *Hfm1*-KO ovaries compared with WT ovaries (Fig. 4d). In summary, these results indicated that HFM1 deficiency affects the formation and stabilization of the ICBs in female germline cysts.

HFM1 is crucial for intercellular bridge function in organelles directional transport

Mammalian oocytes accumulate organelles from sister cells, and several studies have shown that γ-tubulin can be enriched near the intercellular bridge, regulating microtubule-dependent cytoplasmic directional transport [11, 14, 20, 31]. Our results showed that γ-tubulin expression progressively reduced in *Hfm1*-KO germ cells from E17.5 to P3, compared to WT germ cells (Fig. 5a). Statistical analysis suggested that the γ-tubulin foci area of the germ cell was significantly decreased in *Hfm1*-KO mice at E17.5 and P1 (Fig. 5b).

During gametogenesis in female mice, the intercellular bridges begin to appear at E10.5 and dissociate from cytomembrane junctions at E17.5 [18]. In order to exclude the influence of abnormal ICB structure and further clarify the role of HFM1 in ICB function, HFM1 knockdown ovaries were constructed by culturing in vitro with Ad-shRNA-*Hfm1* for 5 days from E17.5 (equaling P3, Fig. 5c). After 5 days of adenovirus transfection, strong green fluorescence was observed under fluorescence microscopy (Fig. 5d), and the protein level of HFM1 was efficiently decreased by Western blotting assay (Fig. 5e). To demonstrate the expression and localization of HFM1, immunofluorescence stained with HFM1 and DDX4 or FOXL2 showed that HFM1 was mainly expressed in the cytoplasm of germ cells (Supplementary Fig. 3a, b). Then, a qRT-PCR assay was performed. Compared with the *Hfm1* mRNA level in E17.5 ovaries, nearly no *Hfm1* mRNA level was detected in KGN cells, primary granulosa cells and HEK 293T cells and a high expression of *Hfm1* mRNA level was observed in oocytes (Supplementary Fig. 3c). Compared with the control group, in which organelles transport within cysts enabled the germ cells to differentiate into primary oocytes, we observed bare

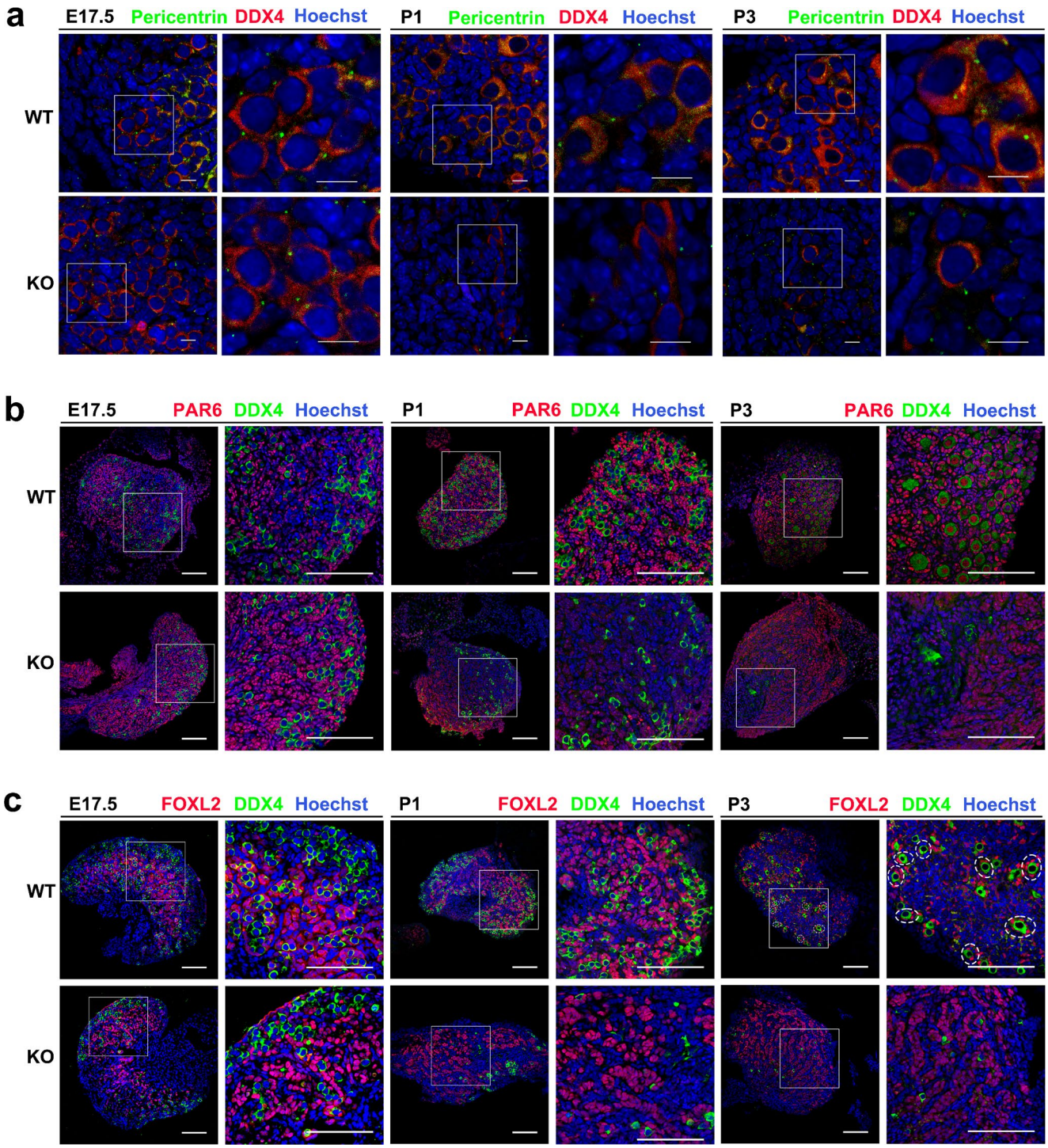

Fig. 3 Depletion of HFM1 affected primordial follicle formation. **a** E17.5, P1, and P3 ovaries stained with Pericentrin (green) to reveal centrosomes. Hoechst (blue) was used to identify the nuclear DNA. Scale bars: 10 μm. **b** Ovaries were stained for DDX4 (green) and PAR6 (red), a potential marker of germ cells for the primordial follicle formation at E17.5, P1, and P3. The nucleus was stained by Hoechst (blue). Scale bars: 100 μm. **c** Immunostaining of WT and *Hfm1*-KO ovaries at E17.5, P1, and P3 using antibodies against DDX4 (green), granulosa cell marker FOXL2 (red), and Hoechst (blue). Primordial follicle (dashed line). Scale bars: 100 μm

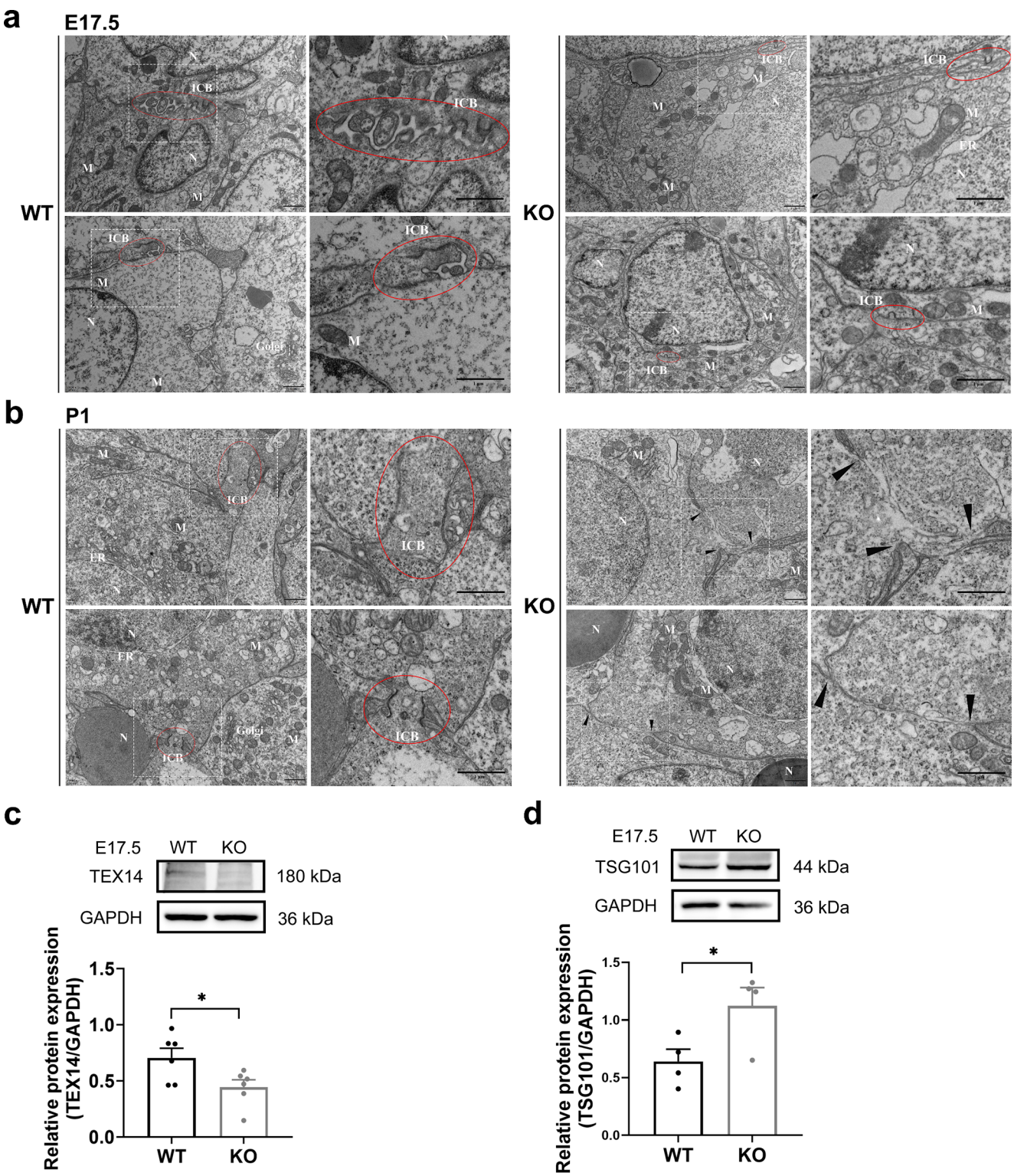

Fig. 4 The formation and stabilization of intercellular bridges were damaged in *Hfm1*-KO mice. **a**, **b** Transmission electron micrograph of the intercellular bridge (ICB, red circle) between germ cells and the plasma membrane gaps (black triangle) in ovaries at E17.5 (a) and P1 (b). Scale bars: 1 μm. **c**, **d** Ovaries in E17.5 WT and *Hfm1*-KO mice. Western blotting was performed to examine the intercellular bridge marker TEX14 (c, unpaired Student's t-test, $n=6$ independent experiments, * $P=0.036$ vs. WT) and the membrane abscission protein TSG101 (d, unpaired Student's t-test, $n=4$ independent experiments, * $P=0.047$ vs. WT). Data are presented as mean ± SEM

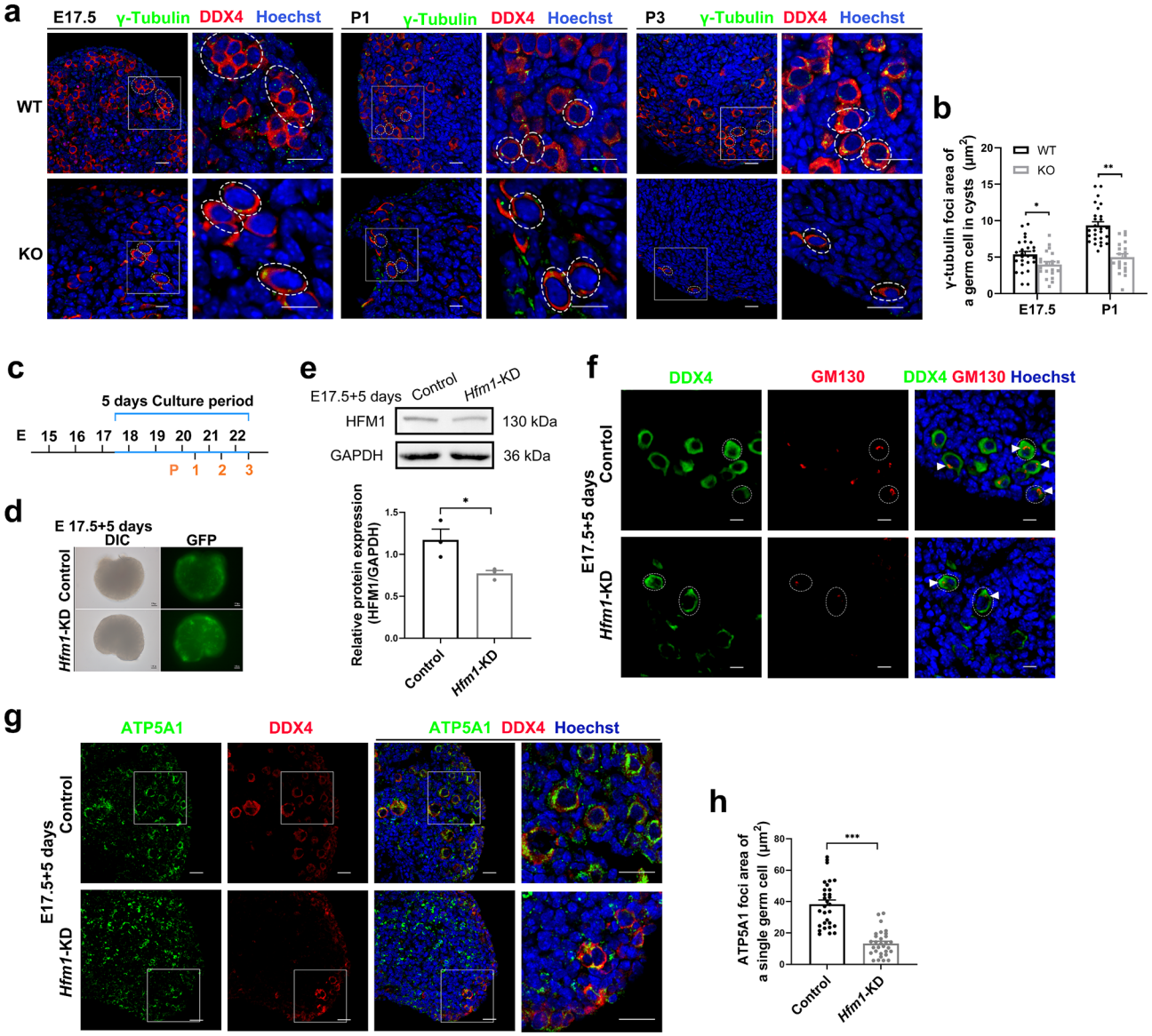

Fig. 5 HFM1 knockdown disturbed the directional organelles transport of intercellular bridge. **a** Immunofluorescence staining for γ-tubulin (green) and DDX4 (red, dash line) at E17.5, P1 and P3. The nucleus was stained by Hoechst (blue). Scale bars: 20 μm. **b** The γ-tubulin foci area of a germ cell in cysts was generated by ImageJ software at E17.5 ($n=26$ for WT and $n=21$ for KO) and P1($n=27$ for WT and $n=20$ for KO) (unpaired Student's t-test, * $P=0.021$, *** $P<0.001$ vs. WT). **c** Timeline showing the 5-day culture scheme. **d** Fluorescence microscope analyses of adenovirus infection efficiency. Strong green fluorescence was observed under the fluorescent microscope following 5 days of adenovirus infection. Scale bars: 100px. **e** Western blotting analysis of HFM1 knockdown efficiency. HFM1 protein expression was down-regulated in Ad-shRNA-*Hfm1* transfected ovaries after 5 days of culture (unpaired Student's t-test, $n=3$ independent experiments, * $P=0.014$ vs. Control). **f** After 5 days of culture, ovaries transfected with Ad-shRNA-*Hfm1* stained with GM130 (red, white triangle) marking Golgi. DDX4 (green) is a germ cell marker. Hoechst (blue) was used to identify the nuclear DNA. Scale bars: 10 μm. **g** E17.5 ovaries were cultured with or without Ad-shRNA-*Hfm1* for 5 days, staining with ATP5A1 (green) and germ cell marker DDX4 (Red). Hoechst (blue) was used to identify the nuclear DNA. Scale bars: 20 μm. **h** The ATP5A1 foci area of a single germ cell was measured by ImageJ software (unpaired Student's t-test, $n=30$, *** $P<0.001$ vs. Control). Data are presented as mean ± SEM

of Golgi complexes and mitochondria enrichment in germ cells by staining with GM130 (white triangle) and ATP5A1 after culturing with Ad-shRNA-*Hfm1* for 5 days (Fig. 5f-h). Taken together, these data suggested that HFM1 is crucial for intercellular bridge function in the directional transport of organelles.

HFM1 regulated the structure and function of ICB through RAC1/ANLN/E-cad signaling pathway

To explore the mechanism of HFM1 in primordial follicle formation, E17.5 mouse ovaries were acquired to perform the co-immunoprecipitation (co-IP) following silver stain,

then HFM1-IP-enriched proteins were analyzed by mass spectroscopy (MS). Totally, 445 candidate targets were identified in our previous work [32]. Rac1 (Ras-related C3 botulinum toxin substrate 1) belongs to the small Rho GTPase family which had a high frequency in MS results. RacGAP1 (Rac GTPase-activating protein) is a vital component of ICB, which stimulates the GTPase activity of RAC1 [33–35]. RAC1 is critical for primordial follicle formation [36], and the interaction between HFM1 and RAC1 was demonstrated by the co-IP assay in ovaries at E17.5 (Fig. 6a). The scaffold protein ANLN (actin-binding protein), localized early to the ICBs, is an F-actin-binding protein that contains a Rho-binding domain [37, 38]. It is reported that the active form of Rho GTPase can directly bind to ANLN and recruit it to the leading edge [39]. Furthermore, our co-IP assay identified the interactions between RAC1 and ANLN in HEK293T cells (Supplementary Fig. 4a). Our results showed that RAC1 and ANLN protein levels were significantly downregulated in *Hfm1*-KO ovaries (Fig. 6b). E-cadherin (E-cad) is a key cell-cell adhesion molecule, which is regulated by RAC1 and CDC42 small G proteins through actin filaments [40, 41]. E-cad junctions between germ cells position intercellular bridges in germ cells [11]. The expression of E-cad was upregulated in *Hfm1*-KO E17.5 ovaries (Fig. 6c), which is consistent with the negative correlation between RAC1 and E-cad expression in somatic cells [42].

To further demonstrate the regulatory network of HFM1 in the function of intercellular bridges, we substantially overexpressed HFM1 in cultured HEK293T cells by transfecting with Flag-HFM1 lentivirus (HFM1-OE). Western blotting detected the transfection efficiency of HFM1 overexpression level in HEK293T cells (Supplementary Fig. 4b). CCK8 assay indicated that the cell viability of the HFM1-OE group was higher than that of the control group (Supplementary Fig. 4c). co-IP assay reidentified that HFM1 and RAC1 have interactions (Fig. 6d). Following animal experiments, we observed the upregulation of RAC1 and ANLN expression and downregulation of E-cad expression in HFM1 overexpression HEK293T cells (Fig. 6e, f). Moreover, we used NSC23766 (a Rac1-specific inhibitor) to inhibit the activity of Rac1 in HEK293T cells transfected with Flag-HFM1 lentivirus (Supplementary Fig. 4d). Our results revealed that NSC23766 treatment repressed the elevated levels of RAC1 and ANLN and reversed the decreased levels of the E-cad induced by HFM1 overexpression (Fig. 6g, h). Collectively, these findings elucidated that HFM1 is associated with ICB in female germline cysts through the RAC1/ANLN/E-cad signaling pathway.

Exogenous RAC1 supplement rescues oocyte differentiation defects caused by HFM1 deletion

We produced and incubated exogenous Ad-shRNA-*Hfm1* and LV-*Rac1* with E17.5 ovaries for 5 days to perform a rescue experiment and the transfection efficiency was confirmed by western blotting and immunofluorescence (Supplementary Fig. 4e, f). The results indicated that the overexpression of RAC1 could rescue the defect in primordial follicle formation (Fig. 7a) induced by HFM1 knockdown. Statistical analysis suggested that RAC1 overexpression improved the knockdown of HFM1-mediated reduction in germ cell number (Fig. 7b) and germ cell area (Fig. 7c). Additionally, the upregulated of E-cad instigated by Ad-shRNA-Hfm1 treatment was effectively attenuated by LV-*Rac1* lentivirus transfection (Fig. 7d). Similarly, the downregulation of RAC1 and ANLN caused by HFM1 knockdown could be partly rescued by RAC1 overexpression (Fig. 7e). On the whole, our findings showed that the overexpression of RAC1 ameliorated the deficiency of oocyte differentiation induced by HFM1 knockdown.

Discussion

Primordial follicles form in the perinatal mammalian ovaries, where pre-granulosa cells enclose single primary oocytes to assemble into the follicular structure [12, 43]. In female cysts, receiving organelles and cytoplasm from sister germ cells via intercellular transport helps the oocyte achieve large volume and preferentially be protected from programmed cell death [12, 18, 20], but its regulation mechanism is still not clear. In this work, we confirmed that HFM1 played an important role in regulating the structure and function of intercellular bridge, and intervening organelle enrichment from sister germ cells, which is imperative for oocyte differentiation and primordial follicle formation.

Stable intercellular bridges are a conserved feature of gametogenesis in multicellular animals observed more than 100 years ago, but their formation and function appear to vary between gender and species. During spermatogenesis in mice, intercellular bridges facilitate the bilateral transfer of signaling molecules between cyst germ cells, enabling synchronized meiosis and symmetrical cell fate in the cyst [25, 44]. Particularly, in oogenesis, intercellular bridges facilitate the directional transfer of the organelle and cytoplasmic transport between sister germ cells, which could induce two asymmetric cell fates: becoming oocytes vs. undergoing cell death. It is reported that *Tex14* mutant male mice were infertility due to a lack of intercellular bridges, but *Tex14* mutant females are still fertile because of persistent cytoplasmic transport between sister germ cells [27, 45].

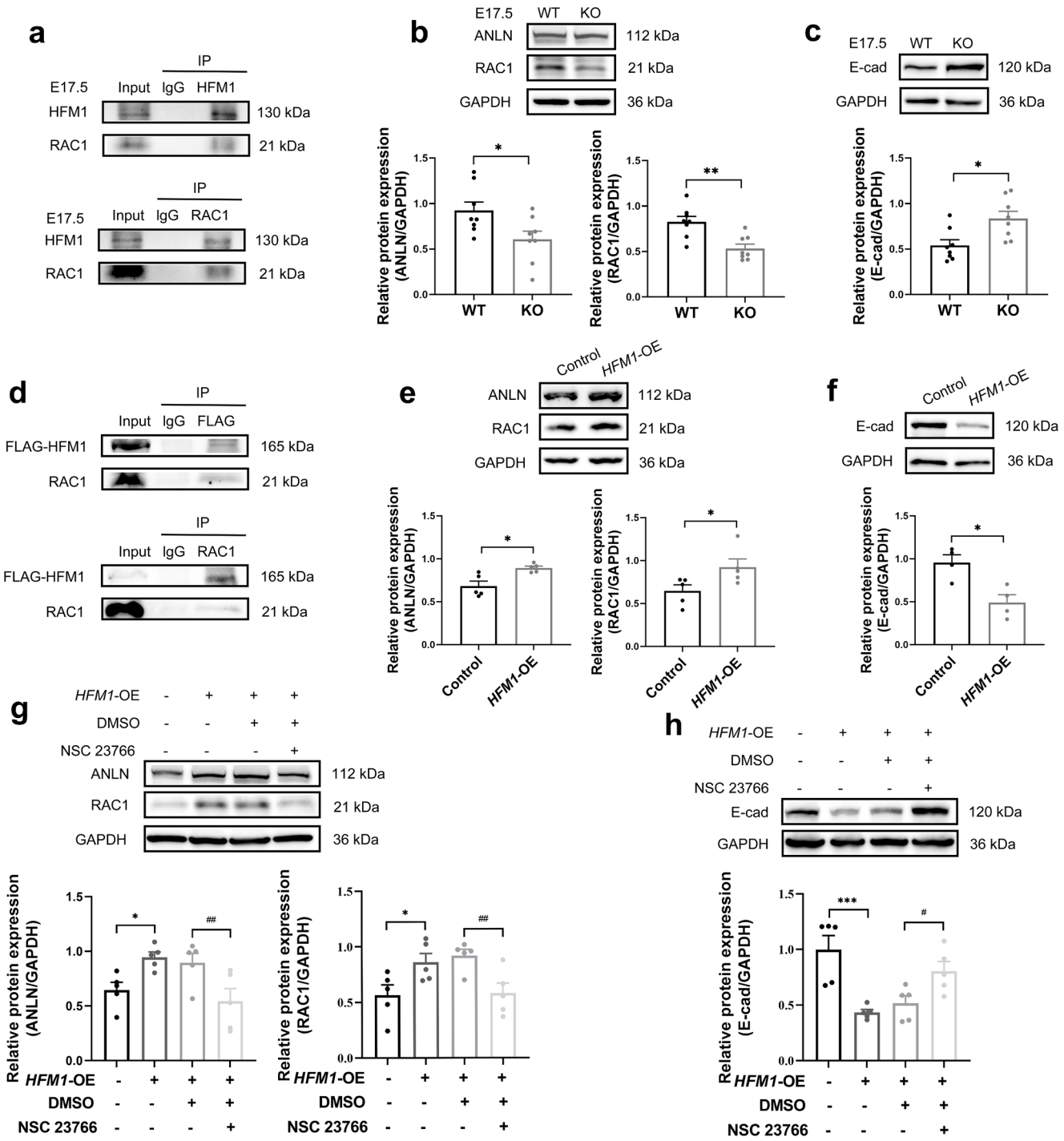

Fig. 6 RAC1/ANLN/E-cad signaling pathway was regulated after knockout or overexpression of HFM1. **a** Co-IP assays depicted that HFM1 interacts with RAC1 in E17.5 ovaries ($n=3$ independent experiments). **b**, **c** Western blotting analysis of RAC1, ANLN, and E-cad protein levels in E17.5 WT and *Hfm1*-KO ovaries. GAPDH served as a loading control (unpaired Student's t-test, $n=8$ independent experiments, * $P=0.029$ or 0.011, ** $P=0.002$ vs. WT). **d** The interaction between HFM1 and RAC1 in HEK293T cells. HEK293T cells were transfected with Flag-*HFM1* lentiviruses for co-IP assays ($n=3$ independent experiments). **e**, **f** RAC1, ANLN, and E-cad protein levels were observed and quantified in HEK293T cells. HEK293T cells were transfected with Flag-*HFM1* lentiviruses for Western blotting assays (unpaired Student's t-test, $n=4$–5 independent experiments, * $P=0.018$ or 0.048 or 0.011 vs. Control). **g**, **h** Western blotting analysis showed that the *Rac1* inhibitor NSC23766 negatived the influence of HFM1 on ANLN and E-cad protein levels (one-way ANOVA, $n=5$ independent experiments, * $P=0.023$ or 0.020, *** $P<0.001$ vs. Control, $^{\#}P=0.029$, $^{\#\#}P=0.009$ or 0.010 vs. *HFM1*-OE + DMSO). Data are presented as mean ± SEM

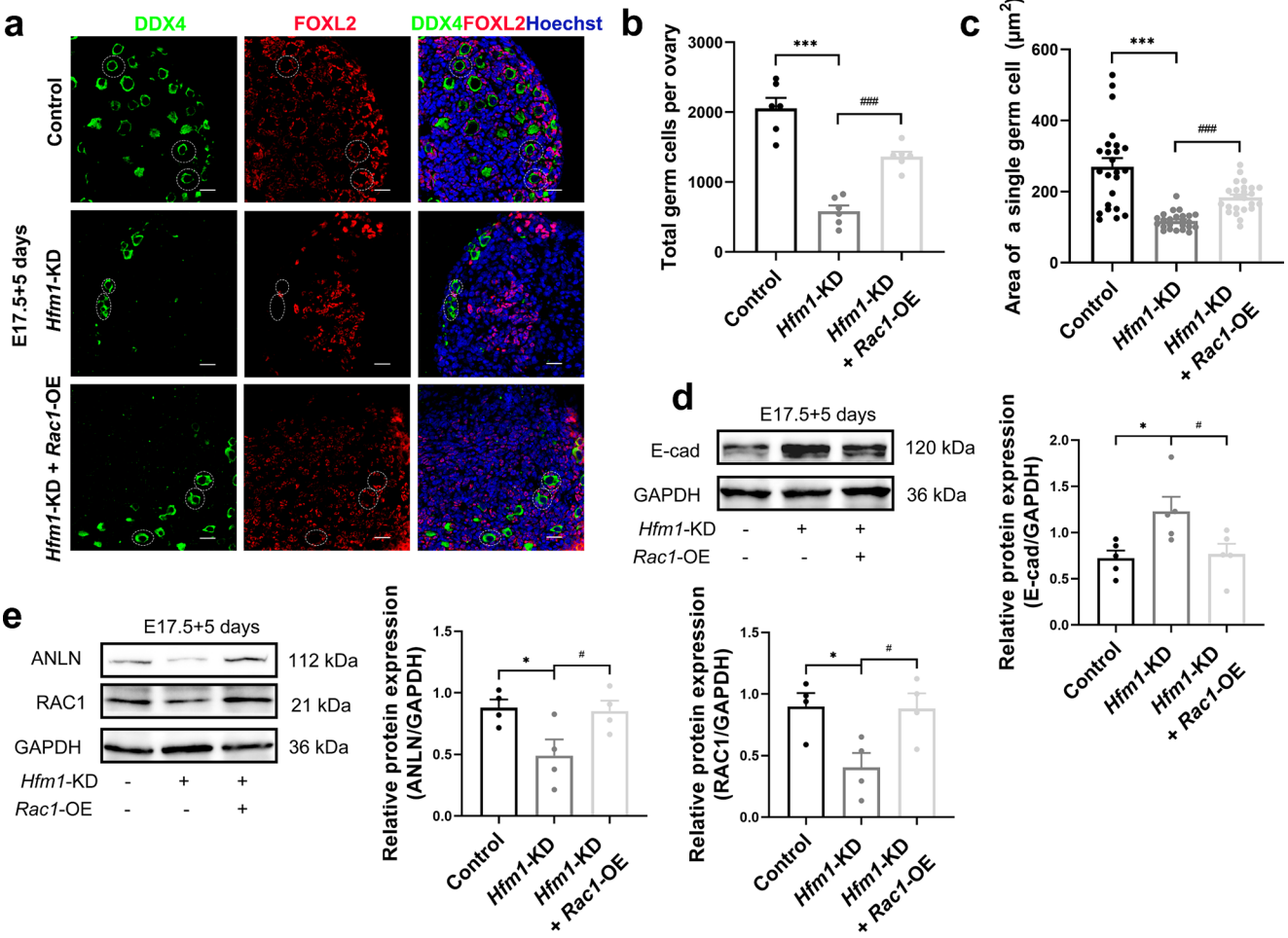

Fig. 7 RAC1 overexpression mitigated the effects of HFM1 knockdown on E17.5 ovaries in vitro. E17.5 ovaries were cultured with Ad-shRNA-*Hfm1* or Ad-shRNA-*Hfm1* plus LV-*Rac1* for 5 days. **a** Ovaries stained with FOXL2 (red) and germ cell marker DDX4 (green). Hoechst (blue) was used to identify the nuclear DNA. Scale bars: 20 μm. **b** Statistical analysis of the numbers of germ cells in ovaries (one-way ANOVA, $n=6$, $^{***}P<0.001$ vs. Control, $^{\#\#\#}P<0.001$ vs. *Hfm*1-KD). **c** The area of a single germ cell was measured by ImageJ in ovaries treated with Ad-shRNA-*Hfm1* or Ad-shRNA-*Hfm1* plus LV-*Rac1* (one-way ANOVA, $n=24$, $^{***}P<0.001$ vs. Control, $^{\#\#\#}P<0.001$ vs. *Hfm*1-KD). **d**, **e** Western blotting analysis of RAC1, ANLN, and E-cad protein levels in ovaries treated with Ad-shRNA-*Hfm1* or Ad-shRNA-*Hfm1* plus LV-*Rac1*(one-way ANOVA, $n=4$–5 independent experiments, * $P=0.012$ or 0.021 or 0.015 vs. Control, $^{\#}P=0.020$ or 0.029 or 0.017 vs. *Hfm*1-KD). Data are presented as mean ± SEM

However, HFM1 deletion alters intercellular bridge formation and function in female germline cysts, which indicates that HFM1 may be a sex-specific intercellular directional transport regulatory factor in ICBs.

The small GTPase family member RAC1 was an important downstream factor of HFM1, which is exclusively expressed in germ cells before follicle assembly and exhibits a decreased level in the oocytes of primordial follicles. In vitro, disruption of RAC1 retards germ cell cyst breakdown, whereas RAC1 overexpression accelerates the formation of primordial follicles [36]. In our results, the expression of RAC1 is regulated by HFM1 in female ovaries, which may mediate organelle transport between sister germ cells. The role of RAC1 in ICBs may also be related to ANLN and E-Cad. Consequently, HFM1 regulated the structure and function of ICB via the RAC1/ANLN/E-cad signaling pathway (Fig. 8). Further structural, function and mechanism studies are necessary to fully demonstrate the definitive role of HFM1 in ICBs during the formation of primordial follicle.

Overall, our studies have provided insight into the distinct roles of HFM1 in oocyte differentiation over the course of primordial follicle formation, with a particular focus on the structure and function of ICBs in female germ cells. However, the selection of primary oocytes and sister germ cells and the ultimate regulation mechanism of cyst-based oocyte production remain imperfectly understood. The regulation of the structure and function of ICBs by HFM1 appears to play a crucial role in primordial follicle formation, which will be fruitful areas for future research and will help us

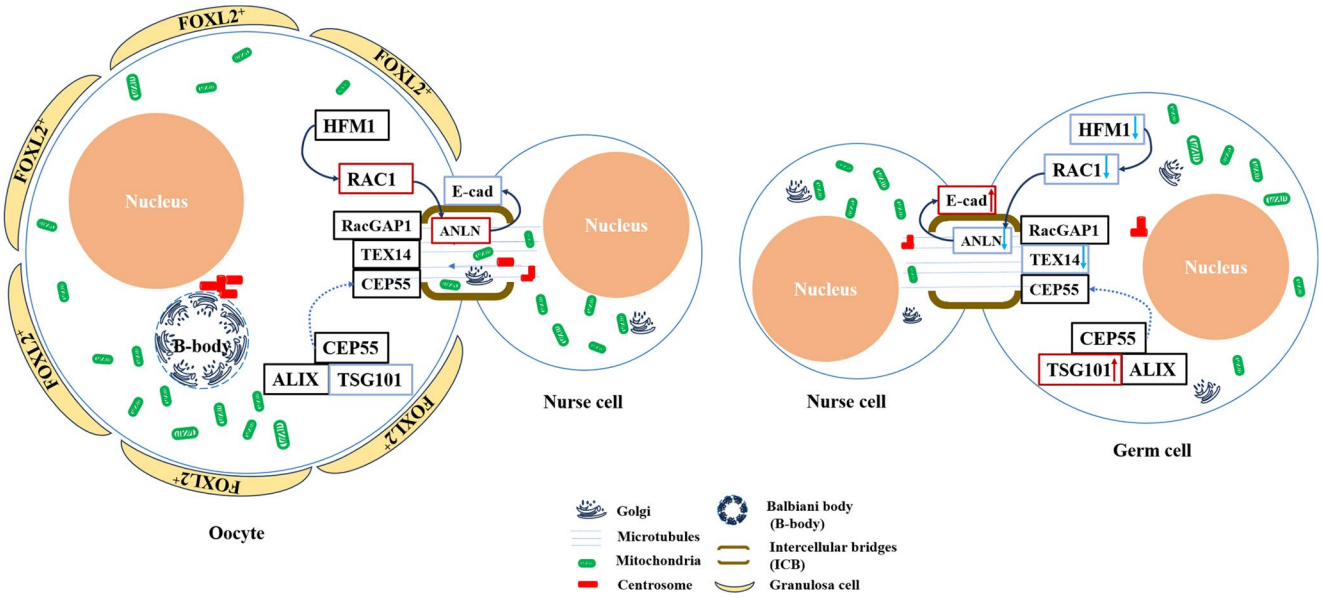

Fig. 8 The schematic illustration of HFM1 regulated germ cell intercellular bridge transport. HFM1 regulated the expression of RAC1 in germ cells, this process impacts ANLN and E-cad expression associated with intercellular bridge and organelle transport, and promotes organelle enrichment and formation of primordial follicles. In *Hfm1*-KO germ cells, deleted level of HFM1 downregulated RAC1, resulting in the defective organelle enrichment in female germline cysts, and the failure of primordial follicles formation

understand the underlying mechanisms that drive oogenesis and ensure female fertility.

Supplementary Information The online version contains supplementary material available at https://doi.org/10.1007/s00018-024-05541-4 .

Author contributions All authors contributed to the study conception and design. YHH, HYW, TTH and LQH carried out the experiments and analyzed the data. CG, LG and YGC provided technical and theoretical help and supervised the study. The first draft of the manuscript was written by YHH and HYW. RRT, DHP and JW contributed to the manuscript revision and discussion. All the authors read the manuscript and approved the final manuscript.

Funding This work was supported by National Natural Science Foundation of China (82471672; 82401920), Natural Science Foundation of Jiangsu Province (BK20241987), Jiangsu Provincial Key Research and Development Program (ZDXK202210), the Jiangsu Innovation Team Project (CXTDA2017004), Young Scholars Research Program of Jiangsu Women and Children Health Hospital (FYRC202011), and the Young Scholars Fostering Fund of the First Affiliated Hospital of Nanjing Medical University (PY2022031).

Data availability Data can be obtained from the corresponding author under reasonable request.

Declarations

Ethics approval Mouse breeding conditions and breeding methods in this experiment strictly complied with the Committee on the Ethics of Animal Experiments of Nanjing Medical University.

Consent to publish All authors read and approved the submission and final publication.

Conflict of interest The authors have no relevant financial or non-financial interests to disclose.

Open Access This article is licensed under a Creative Commons Attribution-NonCommercial-NoDerivatives 4.0 International License, which permits any non-commercial use, sharing, distribution and reproduction in any medium or format, as long as you give appropriate credit to the original author(s) and the source, provide a link to the Creative Commons licence, and indicate if you modified the licensed material. You do not have permission under this licence to share adapted material derived from this article or parts of it. The images or other third party material in this article are included in the article's Creative Commons licence, unless indicated otherwise in a credit line to the material. If material is not included in the article's Creative Commons licence and your intended use is not permitted by statutory regulation or exceeds the permitted use, you will need to obtain permission directly from the copyright holder. To view a copy of this licence, visit http://creativecommons.org/licenses/by-nc-nd/4.0/.

References

1. Telfer EE, Grosbois J, Odey YL, Rosario R, Anderson RA (2023) Making a good egg: human oocyte health, aging, and in vitro development. Physiol Rev 103:2623–2677. https://doi.org/10.1152/physrev.00032.2022
2. Webber L, Davies M, Anderson R, Bartlett J, Braat D, Cartwright B et al (2016) ESHRE Guideline: management of women with premature ovarian insufficiency. Hum Reprod 31:926–937. https://doi.org/10.1093/humrep/dew027
3. Panay N, Anderson RA, Nappi RE, Vincent AJ, Vujovic S, Webber L et al (2020) Premature ovarian insufficiency: an International Menopause Society White Paper. Climacteric 23:426–446. https://doi.org/10.1080/13697137.2020.1804547
4. Huhtaniemi I, Hovatta O, La Marca A, Livera G, Monniaux D, Persani L et al (2018) Advances in the Molecular Pathophysiology, Genetics, and Treatment of Primary Ovarian Insufficiency.

Trends Endocrinol Metab 29:400–419. https://doi.org/10.1016/j.tem.2018.03.010
5. Pu D, Wang C, Cao J, Shen Y, Jiang H, Liu J et al (2016) Association analysis between HFM1 variation and primary ovarian insufficiency in Chinese women. Clin Genet 89:597–602. https://doi.org/10.1111/cge.12718
6. Wang J, Zhang W, Jiang H, Wu BL, Primary Ovarian Insufficiency C (2014) Mutations in HFM1 in recessive primary ovarian insufficiency. N Engl J Med 370:972–974. https://doi.org/10.1056/NEJMc1310150
7. Guiraldelli MF, Eyster C, Wilkerson JL, Dresser ME, Pezza RJ (2013) Mouse HFM1/Mer3 is required for crossover formation and complete synapsis of homologous chromosomes during meiosis. PLoS Genet 9:e1003383. https://doi.org/10.1371/journal.pgen.1003383
8. Wang H, Zhong C, Yang R, Yin Y, Tan R, Gao L et al (2020) Hfm1 participates in Golgi-associated spindle assembly and division in mouse oocyte meiosis. Cell Death Dis 11:490. https://doi.org/10.1038/s41419-020-2697-4
9. Lei L, Spradling AC (2013) Mouse primordial germ cells produce cysts that partially fragment prior to meiosis. Development 140:2075–2081. https://doi.org/10.1242/dev.093864
10. He Y, Chen Q, Dai J, Cui Y, Zhang C, Wen X et al (2021) Single-cell RNA-Seq reveals a highly coordinated transcriptional program in mouse germ cells during primordial follicle formation. Aging Cell 20:e13424. https://doi.org/10.1111/acel.13424
11. Ikami K, Shoffner-Beck S, Tyczynska Weh M, Schnell S, Yoshida S, Diaz Miranda EA et al (2023) Branched germline cysts and female-specific cyst fragmentation facilitate oocyte determination in mice. Proc Natl Acad Sci U S A 120:e2219683120. https://doi.org/10.1073/pnas.2219683120
12. Ikami K, Nuzhat N, Lei L (2017) Organelle transport during mouse oocyte differentiation in germline cysts. Curr Opin Cell Biol 44:14–19. https://doi.org/10.1016/j.ceb.2016.12.002
13. Wang JJ, Ge W, Zhai QY, Liu JC, Sun XW, Liu WX et al (2020) Single-cell transcriptome landscape of ovarian cells during primordial follicle assembly in mice. PLoS Biol 18:e3001025. https://doi.org/10.1371/journal.pbio.3001025
14. Spradling AC, Niu W, Yin Q, Pathak M, Maurya B (2022) Conservation of oocyte development in germline cysts from Drosophila to mouse. https://doi.org/10.7554/eLife.83230. eLife 11
15. Sun YC, Sun XF, Dyce PW, Shen W, Chen H (2017) The role of germ cell loss during primordial follicle assembly: a review of current advances. Int J Biol Sci 13:449–457. https://doi.org/10.7150/ijbs.18836
16. Umeno K, Sasaki A, Kimura N (2022) The impact of oocyte death on mouse primordial follicle formation and ovarian reserve. Reproductive Med biology 21:e12489. https://doi.org/10.1002/rmb2.12489
17. Nguyen DH, Soygur B, Peng SP, Malki S, Hu G, Laird DJ (2020) Apoptosis in the fetal testis eliminates developmentally defective germ cell clones. Nat Cell Biol 22:1423–1435. https://doi.org/10.1038/s41556-020-00603-8
18. Lei L, Spradling AC (2016) Mouse oocytes differentiate through organelle enrichment from sister cyst germ cells. Science 352:95–99. https://doi.org/10.1126/science.aad2156
19. Tingen C, Kim A, Woodruff TK (2009) The primordial pool of follicles and nest breakdown in mammalian ovaries. Mol Hum Reprod 15:795–803. https://doi.org/10.1093/molehr/gap073
20. Niu W, Spradling AC (2022) Mouse oocytes develop in cysts with the help of nurse cells. Cell 185:2576–2590..e2512
21. Pepling ME, Wilhelm JE, O'Hara AL, Gephardt GW, Spradling AC (2007) Mouse oocytes within germ cell cysts and primordial follicles contain a Balbiani body. Proc Natl Acad Sci U S A 104:187–192. https://doi.org/10.1073/pnas.0609923104
22. Wen J, Zhang H, Li G, Mao G, Chen X, Wang J et al (2009) PAR6, a potential marker for the germ cells selected to form primordial follicles in mouse ovary. PLoS ONE 4:e7372. https://doi.org/10.1371/journal.pone.0007372
23. Menendez A, Wanczyk H, Walker J, Zhou B, Santos M, Finck C (2022) Obesity and Adipose Tissue Dysfunction: From Pediatrics to Adults. Genes (Basel) 13. https://doi.org/10.3390/genes13101866
24. Fukuda K, Muraoka M, Kato Y, Saga Y (2021) Decoding the transcriptome of pre-granulosa cells during the formation of primordial follicles in the mouse†. Biol Reprod 105:179–191. https://doi.org/10.1093/biolre/ioab065
25. Greenbaum MP, Iwamori T, Buchold GM, Matzuk MM (2011) Germ cell intercellular bridges. Cold Spring Harb Perspect Biol 3:a005850. https://doi.org/10.1101/cshperspect.a005850
26. Pepling ME, Spradling AC (1998) Female mouse germ cells form synchronously dividing cysts. Development 125:3323–3328. https://doi.org/10.1242/dev.125.17.3323
27. Greenbaum MP, Iwamori N, Agno JE, Matzuk MM (2009) Mouse TEX14 is required for embryonic germ cell intercellular bridges but not female fertility. Biol Reprod 80:449–457. https://doi.org/10.1095/biolreprod.108.070649
28. Iwamori T, Iwamori N, Ma L, Edson MA, Greenbaum MP, Matzuk MM (2010) TEX14 interacts with CEP55 to block cell abscission. Mol Cell Biol 30:2280–2292. https://doi.org/10.1128/mcb.01392-09
29. Kim HJ, Yoon J, Matsuura A, Na JH, Lee WK, Kim H et al (2015) Structural and biochemical insights into the role of testis-expressed gene 14 (TEX14) in forming the stable intercellular bridges of germ cells. Proc Natl Acad Sci U S A 112:12372–12377. https://doi.org/10.1073/pnas.1418606112
30. Pust S, Brech A, Wegner CS, Stenmark H, Haglund K (2023) Vesicle-mediated transport of ALIX and ESCRT-III to the intercellular bridge during cytokinesis. Cell Mol Life Sci 80:235. https://doi.org/10.1007/s00018-023-04864-y
31. Lin H, Yue L, Spradling AC (1994) The Drosophila fusome, a germline-specific organelle, contains membrane skeletal proteins and functions in cyst formation. Development 120:947–956. https://doi.org/10.1242/dev.120.4.947
32. Zhong C, Wang H, Yuan X, He Y, Cong J, Yang R et al (2024) The crucial role of HFM1 in regulating FUS ubiquitination and localization for oocyte meiosis prophase I progression in mice. Biol Res 57:36. https://doi.org/10.1186/s40659-024-00518-w
33. Davies T, Canman JC (2012) Stuck in the middle: Rac, adhesion, and cytokinesis. J Cell Biol 198:769–771. https://doi.org/10.1083/jcb.201207197
34. Touré A, Dorseuil O, Morin L, Timmons P, Jégou B, Reibel L et al (1998) MgcRacGAP, a new human GTPase-activating protein for Rac and Cdc42 similar to Drosophila rotundRacGAP gene product, is expressed in male germ cells. J Biol Chem 273:6019–6023. https://doi.org/10.1074/jbc.273.11.6019
35. Lorès P, Vernet N, Kurosaki T, Van de Putte T, Huylebroeck D, Hikida M et al (2014) Deletion of MgcRacGAP in the male germ cells impairs spermatogenesis and causes male sterility in the mouse. Dev Biol 386:419–427. https://doi.org/10.1016/j.ydbio.2013.12.006
36. Zhao L, Du X, Huang K, Zhang T, Teng Z, Niu W et al (2016) Rac1 modulates the formation of primordial follicles by facilitating STAT3-directed Jagged1, GDF9 and BMP15 transcription in mice. Sci Rep 6:23972. https://doi.org/10.1038/srep23972
37. Sun L, Guan R, Lee IJ, Liu Y, Chen M, Wang J et al (2015) Mechanistic insights into the anchorage of the contractile ring by anillin and Mid1. Dev Cell 33:413–426. https://doi.org/10.1016/j.devcel.2015.03.003
38. Kechad A, Jananji S, Ruella Y, Hickson GR (2012) Anillin acts as a bifunctional linker coordinating midbody ring biogenesis

during cytokinesis. Curr Biol 22:197–203. https://doi.org/10.1016/j.cub.2011.11.062
39. Tian D, Diao M, Jiang Y, Sun L, Zhang Y, Chen Z et al (2015) Anillin Regulates Neuronal Migration and Neurite Growth by Linking RhoG to the Actin Cytoskeleton. Curr Biol 25:1135–1145. https://doi.org/10.1016/j.cub.2015.02.072
40. Izumi G, Sakisaka T, Baba T, Tanaka S, Morimoto K, Takai Y (2004) Endocytosis of E-cadherin regulated by Rac and Cdc42 small G proteins through IQGAP1 and actin filaments. J Cell Biol 166:237–248. https://doi.org/10.1083/jcb.200401078
41. Niu W, Wang Y, Wang Z, Xin Q, Wang Y, Feng L et al (2016) JNK signaling regulates E-cadherin junctions in germline cysts and determines primordial follicle formation in mice. Development 143:1778–1787. https://doi.org/10.1242/dev.132175
42. Li XL, Feng QM, Yang HN, Ruan JW, Kang YF, Yu ZE et al (2022) p120 regulates E-cadherin expression in nasal epithelial cells in chronic rhinosinusitis. Rhinology 60:270–281. https://doi.org/10.4193/Rhin21.276
43. Skinner MK (2005) Regulation of primordial follicle assembly and development. Hum Reprod Update 11:461–471. https://doi.org/10.1093/humupd/dmi020
44. Rezende-Melo CA, Caldeira-Brant AL, Drumond-Bock AL, Buchold GM, Shetty G, Almeida F et al (2020) Spermatogonial asynchrony in Tex14 mutant mice lacking intercellular bridges. Reproduction 160:205–215. https://doi.org/10.1530/rep-20-0118
45. Ikami K, Nuzhat N, Abbott H, Pandoy R, Haky L, Spradling AC et al (2021) Altered germline cyst formation and oogenesis in Tex14 mutant mice. Biol Open 10. https://doi.org/10.1242/bio.058807

Publisher's note Springer Nature remains neutral with regard to jurisdictional claims in published maps and institutional affiliations.